Microscopic study of the fusion reactions ^{40,48}Ca + ^{78}Ni and the effect of the tensor force

Xiang-Xiang Sun (孙向向),[1] Lu Guo (郭璐),[1,2,*] and A. S. Umar[3]

[1]*School of Nuclear Science and Technology, University of Chinese Academy of Sciences, Beijing 100049, China*
[2]*CAS Key Laboratory of Theoretical Physics, Institute of Theoretical Physics, Chinese Academy of Sciences, Beijing 100190, China*
[3]*Department of Physics and Astronomy, Vanderbilt University, Nashville, Tennessee 37235, USA*

(Received 18 January 2022; accepted 18 February 2022; published 1 March 2022)

We provide a microscopic description of the fusion reactions between ^{40,48}Ca and ^{78}Ni. The internuclear potentials are obtained using the density-constrained (DC) time-dependent Hartree-Fock (TDHF) approach and fusion cross sections are calculated via the incoming wave boundary condition method. By performing DC-TDHF calculations at several selected incident energies, the internuclear potentials for both systems are obtained and the energy-dependence of fusion barrier are revealed. The influence of tensor force on internuclear potentials of ^{48}Ca + ^{78}Ni is more obvious than those of ^{40}Ca + ^{78}Ni. By comparing the calculated fusion cross sections between ^{40}Ca + ^{78}Ni and ^{48}Ca + ^{78}Ni, an interesting enhancement of subbarrier fusion cross sections for the former system is found, which can be explained by the narrow width of internuclear potential for ^{40}Ca + ^{78}Ni while the barrier heights and positions are very close to each other. The tensor force suppresses the subbarrier fusion cross sections of both two systems.

DOI: 10.1103/PhysRevC.105.034601

I. INTRODUCTION

Heavy-ion fusion reactions are of particular importance to extend the nuclear chart and for the synthesis of heavy and superheavy elements [1,2]. The development of modern radioactive-ion-beam facilities have greatly broadened our ability to explore the relation between nuclear structure and reaction mechanism [3,4], especially via fusion reactions of exotic nuclei, including weakly bound or halo nuclei and nuclei with a large neutron excess.

The nucleus ^{78}Ni is found to be doubly magic with a large neutron excess ($N - Z$). After its discovery [5], there have been many theoretical and experimental investigations on its structure properties including shell closures at $Z = 28$ and $N = 50$ [6–9], half-life [10–12], energy spectra [13–15], and shape coexistence [16,17]. In a recent investigation on Ni isotopes [18], it has been shown that the tensor part of the Skyrme energy density functional (EDF) significantly affects the spin-orbit splitting of the proton $1f$ orbit, which may explain the endurance of magicity far from the stability valley. This in turn further solidifies the durability of the Skyrme EDF in reproducing the observed shell effects.

But up to now, there has been no theoretical investigation of fusion reactions with ^{78}Ni as reactants, particularly also incorporating the tensor force. To study the influence of neutron excess on fusion, doubly magic nuclei ^{40,48}Ca have been widely used as reactants to study reactions, such as ^{40,48}Ca + ^{90,96}Zr [19–22], ^{40,48}Ca + ^{124,132}Sn [23,24], various Ca + Ca systems [25,26], and ^{40}Ca + ^{58,64}Ni [27], among others. It has been shown that the tensor force also affects the heavy-ion collision process [28–30], the potential barrier, and fusion cross sections [31–33]. Therefore, it is interesting to study the effects of tensor force for the reactions ^{40,48}Ca + ^{78}Ni. To that end, the purpose of the present investigation is to predict the fusion cross sections for ^{40,48}Ca + ^{78}Ni and study the impact of the tensor force on above and below barrier collisions. Study of such reactions may become feasible at modern radioactive-ion-beam facilities in the future.

Most of theoretical approaches used to study the fusion cross sections at both above and below barrier energies have similar starting point, the ion-ion potential. There are mainly two approaches to determine the ion-ion internuclear potential to study fusion reactions: phenomenological ones [34–44] and (semi)microscopic ones [45–57]. Although phenomenological models have been successfully applied to study many aspects of reactions data, their information content is limited due to several adjustable parameters and the absence of dynamics to formulate potentials, such as the Bass model [34], the proximity potential [35,58], the double-folding potential [36], and driven potential from dinuclear system model [37]. The fusion process is particularly complex and the cross section is influenced by many underlying quantal effects. For this reason, it is preferable to use a microscopic model that incorporates the nucleonic degrees of freedom so that the nuclear shell structure and the dynamical effects of the reaction system can be included on the same footing for a more reliable prediction.

The time-dependent Hartree-Fock (TDHF) approach with the mean-field approximation, has been successfully applied to study many aspects of low-energy heavy-ion collisions by calculating the wave functions of nucleons in the three-dimensional grids and considering the structure information of the entrance channel simultaneously (see Refs. [59–63]

*luguo@ucas.ac.cn

and references therein). Because the TDHF theory describes the collective motion in a semiclassical way, the quantum tunneling of the many-body wave function is not included. Therefore, the TDHF theory cannot be directly used to describe subbarrier fusion. The fusion cross sections at above and below barrier energies are usually obtained by solving the Schrödinger equation with ion-ion potentials deduced from TDHF calculations. Several techniques have been developed to obtain internuclear potential within the framework of TDHF, such as frozen HF [64,65], density-constrained (DC) TDHF [50], density-constrained frozen HF [57,66], dissipative-dynamics TDHF [54], and the Thomas-Fermi approximation [51]. Among them, the potentials from the DC-TDHF approach can naturally incorporate all dynamic effects including nucleon transfer, neck formation, internal excitations, deformation effects, and manifestation from the time evolution of the initial configuration. It has been shown in many studies that the calculated fusion cross sections based on the ion-ion potentials with the DC-TDHF approach are generally in good agreement with measurements [31–33,50,55,67–80].

This article is organized as follows: In Sec. II, we show the main theoretical formulation of the DC-TDHF approach. Section III presents the calculational details and the discussion of results. A summary is provided in Sec. IV.

II. THEORETICAL FRAMEWORK

The theoretical framework to calculate the fusion cross section based on the ion-ion potential with the DC-TDHF approach has been presented explicitly in Refs. [3,50,61,69]. Here we introduce the main formulation of this approach for the convenience of discussion. In the TDHF approach, the wave function of the many-body system is approximated as a single Slater determinant composed of single-particle states $\phi_i(\boldsymbol{r})$. With the mean-field approximation, the time evolution of the many-body wave function in the three-dimensional space can be obtained by solving the coupled nonlinear equations for the evolution of the single-particle states,

$$i\hbar\frac{\partial}{\partial t}\phi_i(\boldsymbol{r},t) = h\phi_i(\boldsymbol{r},t), \quad i = 1,\ldots,A, \tag{1}$$

where h is the single-particle Hamiltonian obtained from the Skyrme effective interaction including the contributions from time-odd and tensor components.

Since the TDHF approach does not include the quantum tunneling of the many-body wave function, it cannot be directly applied to study subbarrier fusion reactions. Currently, the fusion reaction is usually treated as a quantum tunneling through an ion-ion potential in the center-of-mass frame. In the DC-TDHF approach, to extract this internuclear potential at certain times during the dynamic evolution, the instantaneous TDHF density $\rho(\boldsymbol{r},t)$ is used to get the static HF minimum energy [50]. This many-body state, $|\Psi_{\rm DC}\rangle$, corresponding to static HF variation process can be obtained by constraining the total density to be equal to the TDHF instantaneous density, corresponding to the internuclear separation, $R(t)$:

$$\delta\langle\Psi_{\rm DC}|H - \int d^3r\lambda(\boldsymbol{r})\rho(\boldsymbol{r},t)|\Psi_{\rm DC}\rangle = 0. \tag{2}$$

The ion-ion potential is then obtained by subtracting the binding energies of projectile and target nuclei, $E_{\rm P}$ and $E_{\rm T}$, respectively,

$$V(R) = \langle\Psi_{\rm DC}|H|\Psi_{\rm DC}\rangle - E_{\rm P} - E_{\rm T}. \tag{3}$$

This approach provides a microscopic internuclear potential starting from Skyrme interactions and there is no additional parameters.

Similarly, the coordinate-dependent mass, $M(R)$, can be obtained using the energy conservation and affects the energy-dependence of potential [77]. For numerical advantages, we use the reduced mass μ and transfer $V(R)$ into a scaled potential $V(\bar{R})$ via a scale transformation

$$d\bar{R} = \left(\frac{M(R)}{\mu}\right)^{1/2} dR. \tag{4}$$

Subsequently, the penetration probabilities $T_L(E_{\rm c.m.})$, corresponding to orbital angular momentum L, are obtained by solving the Schrödinger equation

$$\left[\frac{-\hbar^2}{2\mu}\frac{d^2}{d\bar{R}^2} + \frac{L(L+1)\hbar^2}{2\mu\bar{R}^2} + V(\bar{R}) - E_{\rm c.m.}\right]\psi(\bar{R}) = 0, \tag{5}$$

with the incoming wave boundary-condition method [81]. The fusion cross sections at energies below and above the barrier are then calculated as

$$\sigma_{\rm fus}(E_{\rm c.m.}) = \frac{\pi\hbar^2}{2\mu E_{\rm c.m.}}\sum_{L=0}^{\infty}(2L+1)T_L(E_{\rm c.m.}). \tag{6}$$

III. RESULTS AND DISCUSSIONS

We start our investigations of these reaction systems by performing TDHF calculations with the modified version of the Sky3D code [82] that also incorporates the tensor part of the effective interaction. This code was also used to perform calculations in Refs. [31,32,83–86]. To obtain the ground states of ^{40,48}Ca and ^{78}Ni, the static HF equation are solved on a three-dimensional grid $28 \times 28 \times 28$ fm^3. These three nuclei are all doubly magic and consequently their ground states are spherical. Therefore, pairing correlations can be neglected in both static and dynamic calculations. For the dynamic evolution of central collisions, a three-dimensional grid with the size of $56 \times 40 \times 40$ fm^3 is used and the grid spacing in each direction is taken to be 1 fm. The time step is 0.2 fm/c. The density constraint calculations are performed simultaneously at every 20 time steps (corresponding to a 4 fm/c interval). The initial separation distance of two collision partners is taken to be 20 fm. The convergence property in DC-TDHF calculations is as good as that in the traditional constrained HF with a constraint on a single collective degree of freedom. All the numerical conditions have been checked for achieving a good numerical accuracy for all the cases studied here.

In this work, to explore the effects of tensor force on fusion cross section, the Skyrme interactions SLy5 [87] and SLy5t [88] (SLy5 plus tensor force) are used. These two interactions

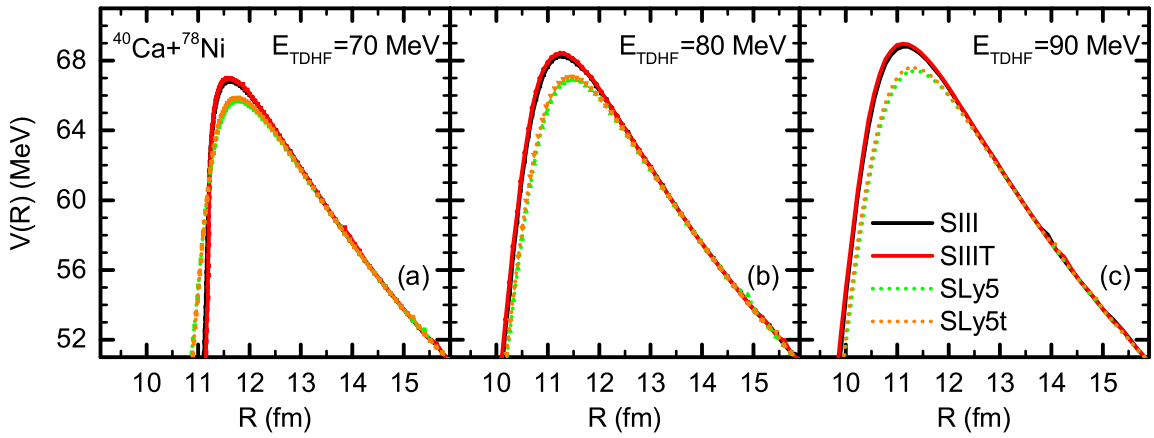

FIG. 1. Internuclear potentials obtained from DC-TDHF calculations for ^{40}Ca + ^{78}Ni at (a) $E_{\rm TDHF} = 70$ MeV, (b) $E_{\rm TDHF} = 80$ MeV, and (c) $E_{\rm TDHF} = 90$ MeV with density functionals SIII, SIIIT, SLy5, and SLy5t.

have been used in many recent investigations with DC-TDHF [31–33,80]. Additionally, in a recent investigation on Ni isotopes [18], by comparing the calculations with SIII interaction [89] and SIII plus tensor force, denoted by SIIIT, it has been shown that the tensor part significantly affects the spin-orbit splitting of the proton $1f$ orbit that may explain the survival of magicity far from the stability valley. Therefore, SIII and SIIIT are also used in the present study on fusion reactions ^{40,48}Ca + ^{78}Ni. The strength of the tensor force is taken to be the same as that given in Ref. [18].

In Figs. 1 and 2, we show the ion-ion potentials for ^{40}Ca + ^{78}Ni and ^{48}Ca + ^{78}Ni from DC-TDHF calculations at incident energies $E_{\rm TDHF} = 70$, 80, and 90 MeV with Skyrme interactions SIII, SIIIT, SLy5, and SLy5t, respectively. As for ^{40}Ca + ^{78}Ni, it is found that the height and position of the fusion barriers calculated by SLy5(t) and SIII(T) differ by about 1.5 MeV and 0.3 fm, respectively. Since the $N(Z) = 20$ shell is spin-saturated while the shells with 28 and 50 are not, the inclusion of the tensor force slightly influences the height and position of the barriers for ^{40}Ca + ^{78}Ni. Although the heights of the barriers increase slowly with the incident energy in DC-TDHF calculations, it is not so dramatic when compared with those in heavy or superheavy systems, such as ^{48}Ca + ^{238}U [90]. For the ^{48}Ca + ^{78}Ni system the effect of the tensor force on barrier heights are more pronounced than those for ^{40}Ca + ^{78}Ni. The inner part of the potential, which affects the subbarrier fusion strongly, shows a more significant change due to the tensor force in ^{48}Ca + ^{78}Ni than ^{40}Ca + ^{78}Ni. This may be partially due to the fact that $N = 28$ shell of ^{48}Ca is spin-unsaturated while the $N(Z) = 20$ shell of ^{40}Ca are spin-saturated. The effects of tensor force on the internuclear potentials of ^{40,48}Ca + ^{78}Ni is similar with the cases of ^{40,48}Ca + ^{48}Ca shown in Ref. [32], in which the effects of tensor force have been discussed explicitly and it is shown that the tensor force influences internuclear potentials with spin-unsaturated systems rather than spin-saturated ones. We also note the more pronounced difference in the barrier widths for the two systems. The effect of this on the fusion cross sections will be discussed below.

The fusion cross sections are calculated by using the transformed ion-ion potentials with the reduced mass μ. Before displaying the fusion cross sections of two reaction systems, we make a comparison of transformed internuclear potentials $V(\bar{R})$ of ^{40}Ca + ^{78}Ni with ^{48}Ca + ^{78}Ni. Since the energy de-

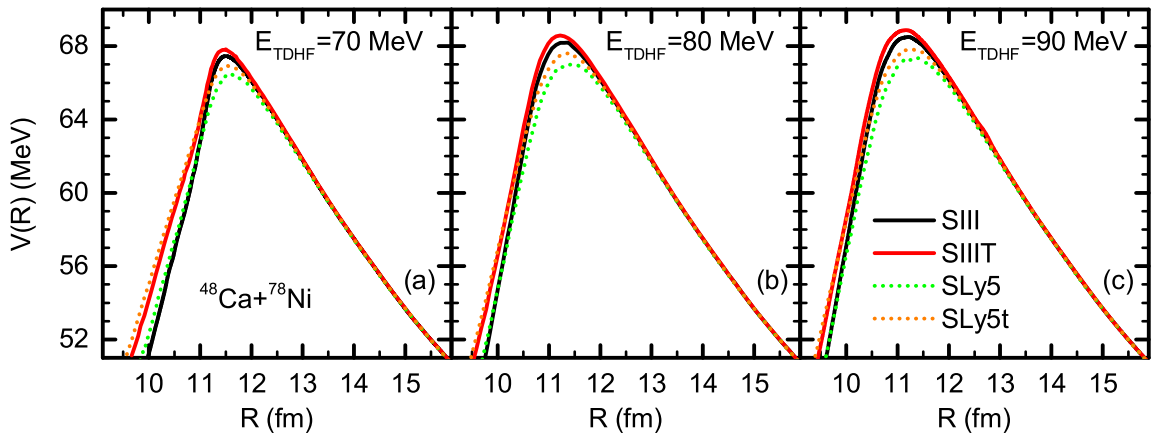

FIG. 2. Internuclear potentials obtained from DC-TDHF calculations for ^{48}Ca + ^{78}Ni at (a) $E_{\rm TDHF} = 70$ MeV, (b) $E_{\rm TDHF} = 80$ MeV, and (c) $E_{\rm TDHF} = 90$ MeV with density functionals SIII, SIIIT, SLy5, and SLy5t.

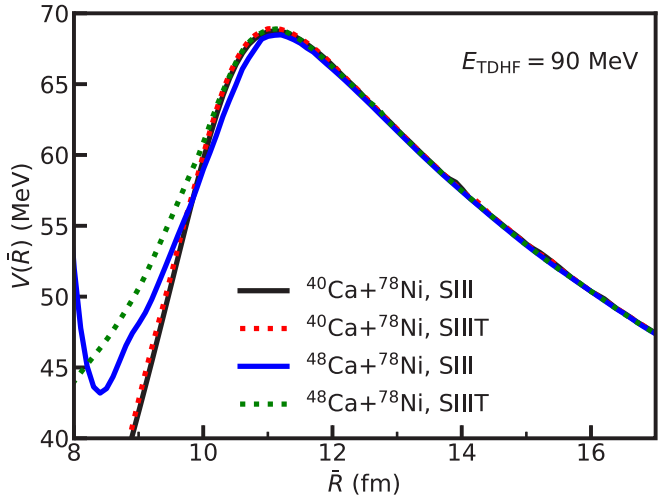

FIG. 3. Transformed internuclear potentials for $^{40}\mathrm{Ca}+^{78}\mathrm{Ni}$ and $^{48}\mathrm{Ca}+^{78}\mathrm{Ni}$ at $E_{\rm TDHF} = 90$ MeV with density functionals SIII and SIIIT.

pendence of potentials from DC-TDHF calculations for both reactions are relatively weak, we show the transformed internuclear potentials with SIII and SIIIT effective interactions at the incident c.m. energy $E_{\rm TDHF} = 90$ MeV in Fig. 3. As a result of the scale transformation, the inner part of the potentials are broadened while the outer region of the potential barrier are unchanged. This is due to the fact that the coordinate-dependent mass changes the interior region of the potential barrier since asymptotically it equals the reduced mass μ and starts to deviate from this in the interior region. Similar conclusions can also be obtained for the potentials calculated with SLy5 and SLy5t, which are shown in Fig. 4. In addition, the difference caused by the tensor force on the inner region is enlarged after the scale transformation, especially for the reaction system $^{48}\mathrm{Ca}+^{78}\mathrm{Ni}$. From Figs. 3 and 4, we see

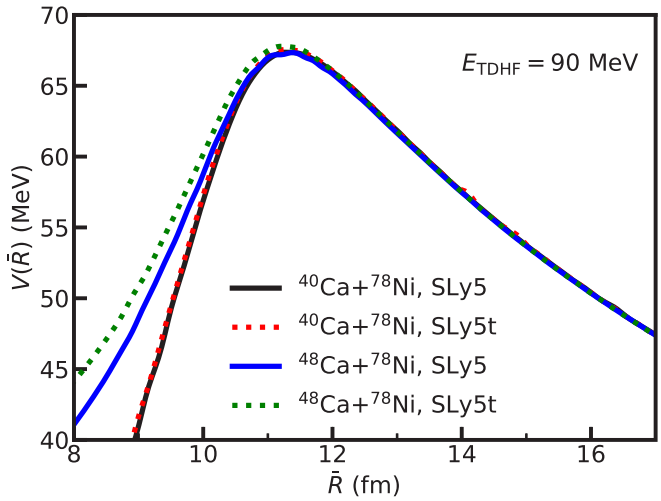

FIG. 4. Transformed internuclear potentials for $^{40}\mathrm{Ca}+^{78}\mathrm{Ni}$ and $^{48}\mathrm{Ca}+^{78}\mathrm{Ni}$ at $E_{\rm TDHF} = 90$ MeV with density functionals SLy5 and SLy5t.

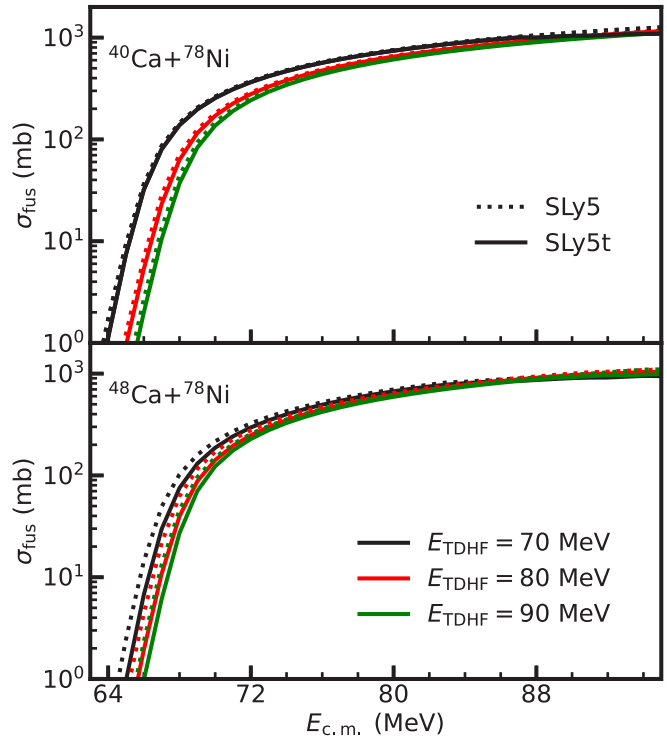

FIG. 5. Fusion cross sections for $^{40}\mathrm{Ca}+^{78}\mathrm{Ni}$ (upper panel) and $^{48}\mathrm{Ca}+^{78}\mathrm{Ni}$ (bottom panel) at $E_{\rm TDHF} = 70$, 80, and 90 MeV, with density functionals SLy5 and SLy5t.

that the position and height of the barriers for $^{40}\mathrm{Ca}+^{78}\mathrm{Ni}$ and $^{48}\mathrm{Ca}+^{78}\mathrm{Ni}$ are very close to each other.

After obtaining the potentials, the fusion cross sections can be calculated for all energies $E_{\rm c.m.}$ in the center-of-mass frame. Usually, if the potentials are strongly dependent on the incident energy $E_{\rm TDHF}$ in TDHF simulations, they should be applied for $E_{\rm c.m.}$ intervals close to a given $E_{\rm TDHF}$ and averaged over an energy interval [76,77]. For the potential of $^{40}\mathrm{Ca}+^{78}\mathrm{Ni}$ with SLy5, the height and position of the barriers change from 65.7 MeV and 11.7 fm at $E_{\rm TDHF} = 70$ MeV to 67.4 MeV and 11.3 fm at $E_{\rm TDHF} = 90$ MeV. The potential of $^{48}\mathrm{Ca}+^{78}\mathrm{Ni}$ with SLy5 at high energy ($E_{\rm TDHF} = 90$ MeV) has a barrier 67.5 MeV located at 11.3 fm, whereas the potential calculated at low energy ($E_{\rm TDHF} = 70$ MeV) has a barrier 66.4 MeV located at 11.6 fm. For potentials with other effective interactions, the changes caused by the $E_{\rm TDHF}$ are similar to the case of SLy5, therefore we do not discuss them in detail. Generally speaking, this energy-dependence of the barrier height and position for $^{40,48}\mathrm{Ca}+^{78}\mathrm{Ni}$ are relatively weak, which is comparable with that for $^{16}\mathrm{O}+^{208}\mathrm{Pb}$ [69]. In present investigation, we calculate the fusion cross section with the potentials at $E_{\rm TDHF} = 70$, 80, and 90 MeV.

Figure 5 shows the calculated fusion cross sections for two reaction systems at different $E_{\rm TDHF}$ with SLy5 and SLy5t, and those with SIII and SIIIT are presented in Fig. 6. First, let us focus on the effects of tensor force. It is found that the fusion cross sections at subbarrier energies are lower after including the tensor force for both two reaction systems and the magnitude of this hindrance for $^{48}\mathrm{Ca}+^{78}\mathrm{Ni}$ is slightly

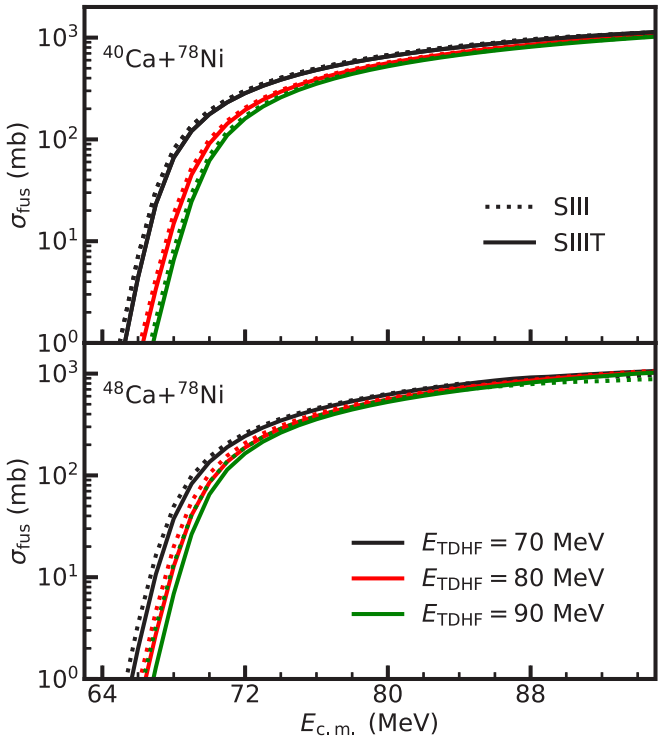

FIG. 6. Fusion cross sections for ^{40}Ca + ^{78}Ni (upper panel) and ^{48}Ca + ^{78}Ni (bottom panel) at $E_{\rm TDHF} = 70$, 80, and 90 MeV, with density functionals SIII and SIIIT.

larger than that for ^{40}Ca + ^{78}Ni. This is due to the tensor force increasing the potential barrier and broadening the inner part the potential. The influence of the tensor force on the fusion cross section and the conclusions obtained in the present case are in line with the conclusions of Ref. [33].

By comparing the fusion cross sections of two reaction systems, it is found that, at subbarrier energies, the fusion cross sections of ^{40}Ca + ^{78}Ni are larger than those of ^{48}Ca + ^{78}Ni by several times, meaning an enhancement of fusion cross sections at subbarrier energies for ^{40}Ca + ^{78}Ni as compared with the more neutron-rich system ^{48}Ca + ^{78}Ni. In our cases, by comparing the internuclear potentials, one observes that the height and position of the barriers for both two systems are almost the same, but the width of ^{40}Ca + ^{78}Ni is narrower than that of ^{48}Ca + ^{78}Ni, resulting in the enhancement of subbarrier fusion cross sections. This situation is similar with the measurements of ^{132}Sn + ^{40}Ca and ^{132}Sn + ^{48}Ca [24]. The enhancement of subbarrier fusion cross sections for ^{132}Sn + ^{40}Ca has also been successfully explained by the DC-TDHF calculations [76] and is due to its narrower width of the ion-ion potential. Additionally, it is should be mentioned that the transfer channels also play an important role for the subbarrier fusion and one can use the particle number projection method [91] to estimate the neutron transfer probabilities. But this is beyond the scope of the present study.

IV. SUMMARY

Doubly magic nucleus ^{78}Ni has a very large neutron excess and its properties are connected with many essential ingredients of nuclear-structure studies, thus drawing many theoretical and experimental interests. In this work, we present the first microscopic study of the fusion reactions involving this nucleus. By using the DC-TDHF approach, the ion-ion potentials of ^{40}Ca + ^{78}Ni and ^{48}Ca + ^{78}Ni are obtained with the only input being the Skyrme effective interactions. By comparing the internuclear potential calculated by SIII (SLy5) with SIIIT (SLy5t), we find that the tensor force increases slightly the potential barrier and broadens the inner part the potential, although the magnitude differs by the system. In addition, the inclusion of the tensor force suppresses the fusion cross sections at subbarrier region. More interesting, it is found that the height and position of the potential barriers for ^{40}Ca + ^{78}Ni and ^{48}Ca + ^{78}Ni are very close to each other while the barrier width of ^{40}Ca + ^{78}Ni is more narrow than that of ^{48}Ca + ^{78}Ni. This results in an enhancement of fusion cross sections of ^{40}Ca + ^{78}Ni at subbarrier energies. The reactions ^{40,48}Ca + ^{78}Ni are expected to be performed at modern radioactive-ion-beam facilities and the predictions presented in this work provide a prior theoretical support.

ACKNOWLEDGMENTS

We thank Shan-Gui Zhou for helpful discussions. This work has been supported by the National Natural Science Foundation of China (Grants No. 11975237, No. 11575189, and No. 11790325) and the Strategic Priority Research Program of Chinese Academy of Sciences (Grant No. XDB34010000 and No. XDPB15) and by the U.S. Department of Energy under Grant No. DE-SC0013847 with Vanderbilt University. The results described in this paper are obtained on the High-performance Computing Cluster of ITP-CAS and the ScGrid of the Supercomputing Center, Computer Network Information Center of Chinese Academy of Sciences.

[1] J. F. Liang and C. Signorini, Fusion induced by radioactive ion beams, Int. J. Mod. Phys. E **14**, 1121 (2005).

[2] G. G. Adamian, N. V. Antonenko, A. Diaz-Torres, and S. Heinz, How to extend the chart of nuclides? Eur. Phys. J. A **56**, 47 (2020).

[3] B. B. Back, H. Esbensen, C. L. Jiang, and K. E. Rehm, Recent developments in heavy-ion fusion reactions, Rev. Mod. Phys. **86**, 317 (2014).

[4] C. L. Jiang, B. B. Back, K. E. Rehm, K. Hagino, G. Montagnoli, and A. M. Stefanini, Heavy-ion fusion reactions at extreme subbarrier energies, Eur. Phys. J. A **57**, 235 (2021).

[5] C. Engelmann, F. Ameil, P. Armbruster, M. Bernas, S. Czajkowski, P. Dessagne, C. Donzaud, H. Geissel, A. Heinz, Z. Janas, C. Kozhuharov, C. Miehe, G. Münzenberg, M. Pfützner, C. Röhl, W. Schwab, C. Stephan, K. Sümmerer, L. Tassan-Got, and B. Voss, Production and identification of heavy Ni

isotopes: Evidence for the doubly magic nucleus $^{78}_{28}$Ni, Z. Phys. A: Hadrons Nucl. **352**, 351 (1995).

[6] J. Hakala, S. Rahaman, V.-V. Elomaa, T. Eronen, U. Hager, A. Jokinen, A. Kankainen, I. D. Moore, H. Penttilä, S. Rinta-Antila, J. Rissanen, A. Saastamoinen, T. Sonoda, C. Weber, and J. Äystö, Evolution of the $N = 50$ Shell Gap Energy Towards ^{78}Ni, Phys. Rev. Lett. **101**, 052502 (2008).

[7] E. Sahin, F. L. Bello Garrote, Y. Tsunoda, T. Otsuka, G. de Angelis, A. Görgen, M. Niikura, S. Nishimura, Z. Y. Xu, H. Baba, F. Browne, M.-C. Delattre, P. Doornenbal, S. Franchoo, G. Gey, K. Hadyńska-Klęk, T. Isobe, P. R. John, H. S. Jung, I. Kojouharov *et al.*, Shell Evolution towards ^{78}Ni: Low-Lying States in ^{77}Cu, Phys. Rev. Lett. **118**, 242502 (2017).

[8] L. Olivier, S. Franchoo, M. Niikura, Z. Vajta, D. Sohler, P. Doornenbal, A. Obertelli, Y. Tsunoda, T. Otsuka, G. Authelet, H. Baba, D. Calvet, F. Château, A. Corsi, A. Delbart, J.-M. Gheller, A. Gillibert, T. Isobe, V. Lapoux, M. Matsushita *et al.*, Persistence of the $Z = 28$ Shell Gap Around ^{78}Ni: First Spectroscopy of ^{79}Cu, Phys. Rev. Lett. **119**, 192501 (2017).

[9] A. Welker, N. A. S. Althubiti, D. Atanasov, K. Blaum, T. E. Cocolios, F. Herfurth, S. Kreim, D. Lunney, V. Manea, M. Mougeot, D. Neidherr, F. Nowacki, A. Poves, M. Rosenbusch, L. Schweikhard, F. Wienholtz, R. N. Wolf, and K. Zuber, Binding Energy of ^{79}Cu: Probing the Structure of the Doubly Magic ^{78}Ni from Only One Proton Away, Phys. Rev. Lett. **119**, 192502 (2017).

[10] P. T. Hosmer, H. Schatz, A. Aprahamian, O. Arndt, R. R. C. Clement, A. Estrade, K.-L. Kratz, S. N. Liddick, P. F. Mantica, W. F. Mueller, F. Montes, A. C. Morton, M. Ouellette, E. Pellegrini, B. Pfeiffer, P. Reeder, P. Santi, M. Steiner, A. Stolz, B. E. Tomlin *et al.*, Half-Life of the Doubly Magic *r*-Process Nucleus ^{78}N i, Phys. Rev. Lett. **94**, 112501 (2005).

[11] Z. Y. Xu, S. Nishimura, G. Lorusso, F. Browne, P. Doornenbal, G. Gey, H.-S. Jung, Z. Li, M. Niikura, P.-A. Söderström, T. Sumikama, J. Taprogge, Z. Vajta, H. Watanabe, J. Wu, A. Yagi, K. Yoshinaga, H. Baba, S. Franchoo, T. Isobe *et al.*, β-Decay Half-Lives of ^{76,77}Co, ^{79,80}Ni, and ^{81}Cu: Experimental Indication of a Doubly Magic ^{78}Ni, Phys. Rev. Lett. **113**, 032505 (2014).

[12] Y. F. Niu, Z. M. Niu, G. Colò, and E. Vigezzi, Interplay of quasiparticle-vibration coupling and pairing correlations on β-decay half-lives, Phys. Lett. B **780**, 325 (2018).

[13] C. Mazzocchi, R. Grzywacz, J. C. Batchelder, C. R. Bingham, D. Fong, J. H. Hamilton, J. K. Hwang, M. Karny, W. Krolas, S. N. Liddick, A. F. Lisetskiy, A. C. Morton, P. F. Mantica, W. F. Mueller, K. P. Rykaczewski, M. Steiner, A. Stolz, and J. A. Winger, Low energy structure of even-even Ni isotopes close to ^{78}Ni, Phys. Lett. B **622**, 45 (2005).

[14] G. Hagen, G. R. Jansen, and T. Papenbrock, Structure of ^{78}Ni from First-Principles Computations, Phys. Rev. Lett. **117**, 172501 (2016).

[15] R. Taniuchi, C. Santamaria, P. Doornenbal, A. Obertelli, K. Yoneda, G. Authelet, H. Baba, D. Calvet, F. Château, A. Corsi, A. Delbart, J.-M. Gheller, A. Gillibert, J. D. Holt, T. Isobe, V. Lapoux, M. Matsushita, J. Menéndez, S. Momiyama, T. Motobayashi *et al.*, ^{78}Ni revealed as a doubly magic stronghold against nuclear deformation, Nature (London) **569**, 53 (2019).

[16] F. Nowacki, A. Poves, E. Caurier, and B. Bounthong, Shape Coexistence in ^{78}Ni as the Portal to the Fifth Island of Inversion, Phys. Rev. Lett. **117**, 272501 (2016).

[17] C. Delafosse, D. Verney, P. Marević, A. Gottardo, C. Michelagnoli, A. Lemasson, A. Goasduff, J. Ljungvall, E. Clément, A. Korichi, G. De Angelis, C. Andreoiu, M. Babo, A. Boso, F. Didierjean, J. Dudouet, S. Franchoo, A. Gadea, G. Georgiev, F. Ibrahim *et al.*, Pseudospin Symmetry and Microscopic Origin of Shape Coexistence in the ^{78}Ni Region: A Hint from Lifetime Measurements, Phys. Rev. Lett. **121**, 192502 (2018).

[18] D. M. Brink and Fl. Stancu, Skyrme density functional description of the double magic ^{78}Ni nucleus, Phys. Rev. C **97**, 064304 (2018).

[19] H. Timmers, L. Corradi, A. M. Stefanini, D. Ackermann, J. H. He, S. Beghini, G. Montagnoli, F. Scarlassara, G. F. Segato, and N. Rowley, Strong isotopic dependence of the fusion of ^{40}Ca + ^{90,96}Zr, Phys. Lett. B **399**, 35 (1997).

[20] H. Timmers, D. Ackermann, S. Beghini, L. Corradi, J. H. He, G. Montagnoli, F. Scarlassara, A. M. Stefanini, and N. Rowley, A case study of collectivity, transfer and fusion enhancement, Nucl. Phys. A **633**, 421 (1998).

[21] A. M. Stefanini, F. Scarlassara, S. Beghini, G. Montagnoli, R. Silvestri, M. Trotta, B. R. Behera, L. Corradi, E. Fioretto, A. Gadea, Y. W. Wu, S. Szilner, H. Q. Zhang, Z. H. Liu, M. Ruan, F. Yang, and N. Rowley, Fusion of ^{48}Ca + ^{90,96}Zr above and below the Coulomb barrier, Phys. Rev. C **73**, 034606 (2006).

[22] A. Stefanini, G. Montagnoli, H. Esbensen, L. Corradi, S. Courtin, E. Fioretto, A. Goasduff, J. Grebosz, F. Haas, M. Mazzocco, C. Michelagnoli, T. Mijatović, D. Montanari, G. Pasqualato, C. Parascandolo, F. Scarlassara, E. Strano, S. Szilner, and D. Torresi, Fusion of ^{40}Ca + ^{96}Zr revisited: Transfer couplings and hindrance far below the barrier, Phys. Lett. B **728**, 639 (2014).

[23] F. Scarlassara, S. Beghini, G. Montagnoli, G. F. Segato, D. Ackermann, L. Corradi, C. J. Lin, A. M. Stefanini, and L. F. Zheng, Fusion of ^{40}Ca + ^{124}Sn around the Coulomb barrier, Nucl. Phys. A **672**, 99 (2000).

[24] J. J. Kolata, A. Roberts, A. M. Howard, D. Shapira, J. F. Liang, C. J. Gross, R. L. Varner, Z. Kohley, A. N. Villano, H. Amro, W. Loveland, and E. Chavez, Fusion of ^{124,132}Sn with ^{40,48}Ca, Phys. Rev. C **85**, 054603 (2012).

[25] C. L. Jiang, A. M. Stefanini, H. Esbensen, K. E. Rehm, L. Corradi, E. Fioretto, P. Mason, G. Montagnoli, F. Scarlassara, R. Silvestri, P. P. Singh, S. Szilner, X. D. Tang, and C. A. Ur, Fusion hindrance for Ca + Ca systems: Influence of neutron excess, Phys. Rev. C **82**, 041601(R) (2010).

[26] G. Montagnoli, A. M. Stefanini, C. L. Jiang, H. Esbensen, L. Corradi, S. Courtin, E. Fioretto, A. Goasduff, F. Haas, A. F. Kifle, C. Michelagnoli, D. Montanari, T. Mijatoviç, K. E. Rehm, R. Silvestri, P. P. Singh, F. Scarlassara, S. Szilner, X. D. Tang, and C. A. Ur, Fusion of ^{40}Ca + ^{40}Ca and other Ca + Ca systems near and below the barrier, Phys. Rev. C **85**, 024607 (2012).

[27] D. Bourgin, S. Courtin, F. Haas, A. M. Stefanini, G. Montagnoli, A. Goasduff, D. Montanari, L. Corradi, E. Fioretto, J. Huiming, F. Scarlassara, N. Rowley, S. Szilner, and T. Mijatović, Barrier distributions and signatures of transfer channels in the ^{40}Ca + ^{58,64}Ni fusion reactions at energies around and below the Coulomb barrier, Phys. Rev. C **90**, 044610 (2014).

[28] S. Fracasso, E. B. Suckling, and P. D. Stevenson, Unrestricted Skyrme-tensor time-dependent Hartree-Fock model and its application to the nuclear response from spherical to triaxial nuclei, Phys. Rev. C **86**, 044303 (2012).

[29] G. Dai, L. Guo, E. Zhao, and S. Zhou, Effect of tensor force on dissipation dynamics in time-dependent Hartree–Fock theory, Sci. China: Phys., Mech. Astron. **57**, 1618 (2014).

[30] P. D. Stevenson, E. B. Suckling, S. Fracasso, M. C. Barton, and A. S. Umar, Skyrme tensor force in heavy ion collisions, Phys. Rev. C **93**, 054617 (2016).

[31] L. Guo, C. Simenel, L. Shi, and C. Yu, The role of tensor force in heavy-ion fusion dynamics, Phys. Lett. B **782**, 401 (2018).

[32] L. Guo, K. Godbey, and A. S. Umar, Influence of the tensor force on the microscopic heavy-ion interaction potential, Phys. Rev. C **98**, 064607 (2018).

[33] K. Godbey, L. Guo, and A. S. Umar, Influence of the tensor interaction on heavy-ion fusion cross sections, Phys. Rev. C **100**, 054612 (2019).

[34] R. Bass, Fusion of heavy nuclei in a classical model, Nucl. Phys. A **231**, 45 (1974).

[35] J. Randrup and J. S. Vaagen, On the proximity treatment of the interaction between deformed nuclei, Phys. Lett. B **77**, 170 (1978).

[36] G. R. Satchler and W. G. Love, Folding model potentials from realistic interactions for heavy-ion scattering, Phys. Rep. **55**, 183 (1979).

[37] G. G. Adamian, N. V. Antonenko, and W. Scheid, Possibilities of synthesis of new superheavy nuclei in actinide–based fusion reactions, Phys. Rev. C **69**, 044601 (2004).

[38] W. J. Świątecki, K. Siwek-Wilczyńska, and J. Wilczyński, Fusion by diffusion. II. Synthesis of transfermium elements in cold fusion reactions, Phys. Rev. C **71**, 014602 (2005).

[39] Z.-Q. Feng, G.-M. Jin, F. Fu, and J.-Q. Li, Production cross sections of superheavy nuclei based on dinuclear system model, Nucl. Phys. A **771**, 50 (2006).

[40] N. Wang, E.-G. Zhao, W. Scheid, and S.-G. Zhou, Theoretical study of the synthesis of superheavy nuclei with $Z = 119$ and 120 in heavy-ion reactions with trans–uranium targets, Phys. Rev. C **85**, 041601(R) (2012).

[41] L. Zhu, W.-J. Xie, and F.-S. Zhang, Production cross sections of superheavy elements $Z = 119$ and 120 in hot fusion reactions, Phys. Rev. C **89**, 024615 (2014).

[42] V. Zagrebaev and W. Greiner, Cross sections for the production of superheavy nuclei, Nucl. Phys. A **944**, 257 (2015).

[43] X. J. Bao, Y. Gao, J. Q. Li, and H. F. Zhang, Possibilities for synthesis of new isotopes of superheavy nuclei in cold fusion reactions, Phys. Rev. C **93**, 044615 (2016).

[44] B. Wang, K. Wen, W.-J. Zhao, E.-G. Zhao, and S.-G. Zhou, Systematics of capture and fusion dynamics in heavy-ion collisions, At. Data Nucl. Data Tables **114**, 281 (2017).

[45] K. A. Brueckner, J. R. Buchler, and M. M. Kelly, New theoretical approach to nuclear heavy-ion scattering, Phys. Rev. **173**, 944 (1968).

[46] A. Diaz Torres, G. G. Adamian, N. V. Antonenko, and W. Scheid, Potential in mass asymmetry and quasifission in a dinuclear system, Nucl. Phys. A **679**, 410 (2001).

[47] P. Möller, A. J. Sierk, and A. Iwamoto, Five–Dimensional Fission–Barrier Calculations from ^{70}Se to ^{252}Cf, Phys. Rev. Lett. **92**, 072501 (2004).

[48] L. Guo, F. Sakata, and E.-G. Zhao, Characteristic feature of self–consistent mean–field in level crossing region, Nucl. Phys. A **740**, 59 (2004).

[49] L. Guo, F. Sakata, and E.-G. Zhao, Applicability of self–consistent mean–field theory, Phys. Rev. C **71**, 024315 (2005).

[50] A. S. Umar and V. E. Oberacker, Heavy-ion interaction potential deduced from density-constrained time-dependent Hartree-Fock calculation, Phys. Rev. C **74**, 021601(R) (2006).

[51] N. Wang, X. Wu, Z. Li, M. Liu, and W. Scheid, Applications of Skyrme energy-density functional to fusion reactions for synthesis of superheavy nuclei, Phys. Rev. C **74**, 044604 (2006).

[52] Ş. Mişicu and H. Esbensen, Signature of shallow potentials in deep sub-barrier fusion reactions, Phys. Rev. C **75**, 034606 (2007).

[53] A. Diaz-Torres, L. R. Gasques, and M. Wiescher, Effects of nuclear molecular configurations on the astrophysical S-factor for $^{16}\mathrm{O} + {}^{16}\mathrm{O}$, Phys. Lett. B **652**, 255 (2007).

[54] K. Washiyama and D. Lacroix, Energy dependence of the nucleus-nucleus potential close to the Coulomb barrier, Phys. Rev. C **78**, 024610 (2008).

[55] C. Simenel, R. Keser, A. S. Umar, and V. E. Oberacker, Microscopic study of $^{16}\mathrm{O} + {}^{16}\mathrm{O}$ fusion, Phys. Rev. C **88**, 024617 (2013).

[56] K. Wen, F. Sakata, Z.-X. Li, X.-Z. Wu, Y.-X. Zhang, and S.-G. Zhou, Non-Gaussian Fluctuations and Non-Markovian Effects in the Nuclear Fusion Process: Langevin Dynamics Emerging from Quantum Molecular Dynamics Simulations, Phys. Rev. Lett. **111**, 012501 (2013).

[57] C. Simenel, A. S. Umar, K. Godbey, M. Dasgupta, and D. J. Hinde, How the Pauli exclusion principle affects fusion of atomic nuclei, Phys. Rev. C **95**, 031601(R) (2017).

[58] M. Seiwert, W. Greiner, V. Oberacker, and M. J. Rhoades-Brown, Test of the proximity theorem for deformed nuclei, Phys. Rev. C **29**, 477 (1984).

[59] C. Simenel, Nuclear quantum many-body dynamics, Eur. Phys. J. A **48**, 152 (2012).

[60] T. Nakatsukasa, K. Matsuyanagi, M. Matsuo, and K. Yabana, Time-dependent density-functional description of nuclear dynamics, Rev. Mod. Phys. **88**, 045004 (2016).

[61] C. Simenel and A. S. Umar, Heavy-ion collisions and fission dynamics with the time–dependent Hartree-Fock theory and its extensions, Prog. Part. Nucl. Phys. **103**, 19 (2018).

[62] P. D. Stevenson and M. C. Barton, Low–energy heavy-ion reactions and the Skyrme effective interaction, Prog. Part. Nucl. Phys. **104**, 142 (2019).

[63] K. Sekizawa, TDHF theory and its extensions for the multi-nucleon transfer reaction: A mini review, Front. Phys. **7**, 20 (2019).

[64] L. Guo and T. Nakatsukasa, Time-dependent Hartree-Fock studies of the dynamical fusion threshold, EPJ Web Conf. **38**, 09003 (2012).

[65] D. Bourgin, C. Simenel, S. Courtin, and F. Haas, Microscopic study of $^{40}\mathrm{Ca} + {}^{58,64}\mathrm{Ni}$ fusion reactions, Phys. Rev. C **93**, 034604 (2016).

[66] A. S. Umar, C. Simenel, and K. Godbey, Pauli energy contribution to the nucleus-nucleus interaction, Phys. Rev. C **104**, 034619 (2021).

[67] A. S. Umar and V. E. Oberacker, Time dependent Hartree-Fock fusion calculations for spherical, deformed systems, Phys. Rev. C **74**, 024606 (2006).

[68] A. S. Umar and V. E. Oberacker, $^{64}\mathrm{Ni} + {}^{64}\mathrm{Ni}$ fusion reaction calculated with the density-constrained time-dependent Hartree-Fock formalism, Phys. Rev. C **77**, 064605 (2008).

[69] A. S. Umar and V. E. Oberacker, Density-constrained time-dependent Hartree-Fock calculation of $^{16}\mathrm{O} + {}^{208}\mathrm{Pb}$ fusion cross-sections, Eur. Phys. J. A **39**, 243 (2009).

[70] A. S. Umar, V. E. Oberacker, J. A. Maruhn, and P.-G. Reinhard, Microscopic calculation of precompound excitation energies for heavy-ion collisions, Phys. Rev. C **80**, 041601(R) (2009).
[71] A. S. Umar, J. A. Maruhn, N. Itagaki, and V. E. Oberacker, Microscopic Study of the Triple-α Reaction, Phys. Rev. Lett. **104**, 212503 (2010).
[72] V. E. Oberacker, A. S. Umar, J. A. Maruhn, and P.-G. Reinhard, Microscopic study of the ^{132,124}Sn + ^{96}Zr reactions: Dynamic excitation energy, energy-dependent heavy-ion potential, and capture cross section, Phys. Rev. C **82**, 034603 (2010).
[73] R. Keser, A. S. Umar, and V. E. Oberacker, Microscopic study of Ca + Ca fusion, Phys. Rev. C **85**, 044606 (2012).
[74] A. S. Umar, V. E. Oberacker, and C. J. Horowitz, Microscopic sub-barrier fusion calculations for the neutron star crust, Phys. Rev. C **85**, 055801 (2012).
[75] C. Simenel, M. Dasgupta, D. J. Hinde, and E. Williams, Microscopic approach to coupled-channels effects on fusion, Phys. Rev. C **88**, 064604 (2013).
[76] V. E. Oberacker and A. S. Umar, Microscopic analysis of sub-barrier fusion enhancement in ^{132}Sn + ^{40}Ca versus ^{132}Sn + ^{48}Ca, Phys. Rev. C **87**, 034611 (2013).
[77] A. S. Umar, C. Simenel, and V. E. Oberacker, Energy dependence of potential barriers and its effect on fusion cross sections, Phys. Rev. C **89**, 034611 (2014).
[78] A. S. Umar and V. E. Oberacker, Time-dependent HF approach to SHE dynamics, Nucl. Phys. A **944**, 238 (2015).
[79] A. S. Umar, V. E. Oberacker, and C. Simenel, Fusion and quasifission dynamics in the reactions ^{48}Ca + ^{249}Bk and ^{50}Ti + ^{249}Bk using a time-dependent Hartree-Fock approach, Phys. Rev. C **94**, 024605 (2016).
[80] K. Godbey, C. Simenel, and A. S. Umar, Absence of hindrance in microscopic ^{12}C + ^{12}C fusion study, Phys. Rev. C **100**, 024619 (2019).
[81] K. Hagino, N. Rowley, and A. T. Kruppa, A program for coupled-channel calculations with all order couplings for heavy-ion fusion reactions, Comput. Phys. Commun. **123**, 143 (1999).
[82] J. A. Maruhn, P.-G. Reinhard, P. D. Stevenson, and A. S. Umar, The TDHF Code Sky3D, Comput. Phys. Commun. **185**, 2195 (2014).
[83] G.-F. Dai, L. Guo, E.-G. Zhao, and S.-G. Zhou, Dissipation dynamics and spin–orbit force in time–dependent Hartree–Fock theory, Phys. Rev. C **90**, 044609 (2014).
[84] L. Guo, C. Shen, C. Yu, and Z. Wu, Isotopic trends of quasifission and fusion-fission in the reactions ^{48}Ca + ^{239,244}Pu, Phys. Rev. C **98**, 064609 (2018).
[85] Z. Wu and L. Guo, Microscopic studies of production cross sections in multinucleon transfer reaction ^{58}Ni + ^{124}Sn, Phys. Rev. C **100**, 014612 (2019).
[86] Z. Wu and L. Guo, Production of proton-rich actinide nuclei in the multinucleon transfer reaction ^{58}Ni + ^{232}Th, Sci. China: Phys., Mech. Astron. **63**, 242021 (2020).
[87] E. Chabanat, P. Bonche, P. Haensel, J. Meyer, and R. Schaeffer, A Skyrme parametrization from subnuclear to neutron star densities Part II. Nuclei far from stabilities, Nucl. Phys. A **635**, 231 (1998).
[88] G. Colò, H. Sagawa, S. Fracasso, and P. F. Bortignon, Spin–orbit splitting and the tensor component of the Skyrme interaction, Phys. Lett. B **646**, 227 (2007).
[89] M. Beiner, H. Flocard, N. V. Giai, and P. Quentin, Nuclear ground-state properties and self-consistent calculations with the Skyrme interaction: (I). Spherical description, Nucl. Phys. A **238**, 29 (1975).
[90] A. S. Umar, V. E. Oberacker, J. A. Maruhn, and P.-G. Reinhard, Entrance channel dynamics of hot and cold fusion reactions leading to superheavy elements, Phys. Rev. C **81**, 064607 (2010).
[91] C. Simenel, Particle Transfer Reactions with the Time-Dependent Hartree-Fock Theory Using a Particle Number Projection Technique, Phys. Rev. Lett. **105**, 192701 (2010).